

Transients control in Raman fiber amplifiers

Marcio Freitas ^{a b}, Sidney Givigi Jr ^{ab}, Jackson Klein ^a, Luiz C. Calmon ^b, Ailson R. de Almeida ^b

^a Optiwave Corporation, 7 Capella Court, Ottawa, Ontario, K2E 7X1, Canada

^b Dep. of Electrical Engineering, Univ. Federal do Espírito Santo, Caixa Postal 01-9011, Vitória, ES, Brazil, CEP 29060-970

ABSTRACT

Raman fiber amplifiers (RFA) are being used in optical transmission communication systems in the recent years due to their advantages in comparison to erbium-doped fiber amplifiers (EDFA). Recently the analysis of RFAs dynamic response and transients control has become important in order to predict the system response to add/drop of channels or cable cuts in optical systems, and avoid impairments caused by the power transients. Fast signal power transients in the surviving channels are caused by the cross-gain saturation effect in RFA and the slope of the gain saturation characteristics determines the steady-state surviving channel power excursion. We are presenting the modeling and analysis of power transients and its control using a pump control method for a single and multi-pump scheme.

Keywords: Raman fiber amplifier, Power transients

1. INTRODUCTION

For the past few years, research on Raman fiber amplifiers has been boosted due to the advantages they have over erbium-doped fiber amplifiers, such as the existence of Raman gain in every fiber, the availability of gain over the entire transparency region of the fiber, the fact that the gain spectrum of Raman amplifiers may be tailored by adjusting the pump wavelength configuration, improved noise figure, and reduced nonlinear penalty [1]. One of the biggest concerns in using rare-earth fiber amplifiers for optical WDM networking is that networks become vulnerable to transient inter-channel cross-gain modulation while undergoing dynamic configurations [2, 3]. Since optical amplifiers in general, and RFAs in particular, saturate on a total-power basis, addition and/or removal of channels in a WDM network may disturb channels at other wavelengths that share the same path, causing power transients in the surviving channels that could result in serious service impairment [2]. For this reason, a control scheme that reduces power transients and protects surviving channels is necessary.

Several papers are particularly focused on analyzing the dynamic behavior of RFAs and the power transients in surviving channels [4-6]. Simulations have demonstrated consistency with experimental results, and add/drop of channels or cable cuts have been studied for co-pumped and counter-pumped configurations. The observed differences between the steady-state gain and the gain in the surviving channels after some of the channels are dropped can cause serious impairment, and therefore must be predicted in order to implement control systems that avoid such phenomena. The objective of this article is to develop a procedure to obtain and tune controllers independently of specific systems characteristics.

Section 2 presents the numerical modeling for simulation of dynamic events in RFAs. Section 3 presents the structure of an auto-tuning scheme for PD controllers by using genetic algorithms. Section 4 presents simulation results for cases wherein one and two counter-directionally pumps are used.

2. NUMERICAL MODEL

The numerical model used to describe the dynamic behavior of a RFA is based on the one derived in [6]. The physical effects taken into account in this model are:

- Pump-to-pump, signal-to-signal, and pump-to-signal Raman interactions;

- Spontaneous Raman emission and its temperature dependency;
- Stimulated Raman scattering;
- Pump depletions due to Raman energy transfer;
- High-order Stokes generation;
- Multiple Rayleigh backscattering;
- Fiber loss dependent on the wavelength.

When all these effects are considered, the propagation equations describing the forward and backward power evolutions are written in the following form:

$$\begin{aligned}
\frac{\partial P^\pm(z, t, \mathbf{u})}{\partial z} \mu \frac{1}{V_g(\mathbf{u})} \frac{\partial P^\pm(z, t, \mathbf{u})}{\partial t} &= \mu \mathbf{a}(\mathbf{u}) P^\pm(z, t, \mathbf{u}) \pm \mathbf{g}(\mathbf{u}) P^\mu(z, t, \mathbf{u}) \pm \\
&P^\pm(z, t, \mathbf{u}) \sum_{\mathbf{n} < \mathbf{V}} \frac{g_r(\mathbf{u} - \mathbf{V})}{K_{eff} A_{eff}} [P^\pm(z, t, \mathbf{V}) + P^\mu(z, t, \mathbf{V})] \pm \\
&h \Delta \mathbf{u} \sum_{\mathbf{u} < \mathbf{V}} \frac{g_r(\mathbf{u} - \mathbf{V})}{A_{eff}} [P^\pm(z, t, \mathbf{V}) + P^\mu(z, t, \mathbf{V})] \left[1 + \left(\exp \left[\frac{h(\mathbf{V} - \mathbf{u})}{kT} \right] - 1 \right)^{-1} \right] \mu \quad (1) \\
&P^\pm(z, t, \mathbf{u}) \sum_{\mathbf{u} > \mathbf{V}} \frac{g_r(\mathbf{u} - \mathbf{V})}{K_{eff} A_{eff}} \frac{\mathbf{u}}{\mathbf{V}} [P^\pm(z, t, \mathbf{V}) + P^\mu(z, t, \mathbf{V})] \mu \\
&2h \mathbf{u} \Delta \mathbf{u} P^\pm(z, t, \mathbf{u}) \sum_{\mathbf{u} > \mathbf{V}} \frac{g_r(\mathbf{u} - \mathbf{V})}{A_{eff}} \left[1 + \left(\exp \left[\frac{h(\mathbf{u} - \mathbf{V})}{kT} \right] - 1 \right)^{-1} \right]
\end{aligned}$$

where ω, ζ are the wave frequencies [Hz], $P^+(z, t, \mathbf{u})$ is the forward power of signal (pump) at frequency ω [W], $P^-(z, t, \mathbf{u})$ is the backward power of signal (pump) at frequency ω [W], $V_g(\mathbf{u})$ is the frequency-dependent group velocity, $\alpha(\omega)$ is the fiber attenuation [N/m], $\gamma(\nu)$ is the Rayleigh backscattering coefficient [N/m], $g_r(\nu - \zeta)$ is the Raman gain coefficient for frequency difference $(\omega - \zeta)$ [m/W], A_{eff} is effective area [m²], K_{eff} is polarization factor, $\Delta \omega$ is the frequency interval [Hz], h is the Plank's constant, k is the Boltzman's constant, and T the absolute temperature of the fiber [K].

For the solution of (1), the steady-state solution is found through the application of the fourth-order Runge-Kutta. This first result consolidates the longitudinal distribution of all individual powers (pumps, signals, ASE waves) along the fiber. Then, this solution is directly integrated, [7] and the time evolution of pumps, signals, and ASE waves is determined. In order to guarantee that the solution in time domain does not present undesirable oscillations, the bin widths in space (Δz) and time (Δt) must be chosen carefully. The stable solution has been obtained [1] when the time bin Δt is equal to or smaller than the propagation time through the space bin, i.e., $\Delta t \leq \Delta z / V_g$.

The Raman gain coefficients used in this work are calculated based on the normalized gain profile shown in Fig. 1. As shown in [10] and [11] the normalized profiles are very similar even for different fibers such as standard single-mode fibers (SMF), dispersion-shift fibers (DSF), and dispersion-compensation fiber (DCF). The slight differences can be neglected without losing accuracy. Therefore, this normalized Raman gain profile is considered the same for all fibers used here and the Raman gain coefficients are calculated in accordance with:

$$g_r(\nu) = G_r \cdot g_{rNor}(\nu) \cdot \frac{\nu_{pump}}{\nu_{ref}} \quad (2)$$

Where G_r is the Raman gain peak for the reference pump frequency, $\nu_{ref} \cdot g_{rNor}(\nu)$ is the normalized Raman gain coefficient, see Fig. 1, and ν_{pump} is pump frequency.

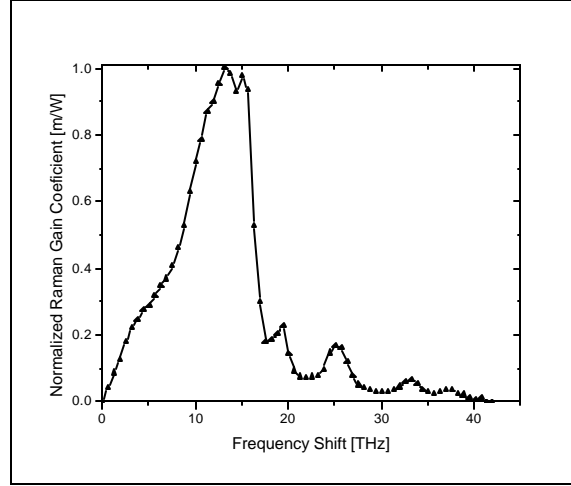


Figure 1 - Normalized Raman Gain Coefficient for silica fiber

3. CONTROLLER TUNING

As described in the numerical model section, the numerical solving of the equation (1) is carried out in two steps: the first for the steady-state and the second for the time integration. Once the first step is complete, the second one (where the control loop is performed) can be rewritten as:

$$\dot{p} = Ap + Bu \quad (3)$$

where p is the power for each signal, A is related to the steady-state power distribution, B is the control matrix, and u is the new input on time for each channel being propagated in the fiber.

Assuming that a PID controller does not give a satisfactory result [2], and since the only inputs that can be controlled are the pumps, the feedback-loop may be closed by using:

$$\dot{p}_{pump} = p_{pump} - (K_P (p_{sur} - p_0) + K_D \dot{p}_{sur}) \quad (4)$$

where p_{pump} is the pump channels, p_{sur} is the power of the surviving channel chosen at the time t considered, p_0 is the power of the surviving channel at steady-state, and K_D and K_P are the gains of the proportional and differential errors used in the feedback control loop.

If we restate the problem above, the requirement is to find the coefficient matrices K_D and K_P in order to minimize the transient for the surviving channels in general and, specifically, for the surviving channel chosen to monitor the control strategy. Karásek and Menif [2], proposed a procedure based on the Ziegler-Nichols method [8] to solve this problem. However, two other problems arise from the solution they proposed. Firstly, it is necessary to have a complete, in-depth knowledge of the characteristics of the system to be controlled. Secondly, it appears to work just for one pump. Since most current systems work with multiple pumps, this last problem becomes critical.

To address these stated issues, we used genetic algorithms to obtain the gain matrices K_D and K_P . The following two objectives are stated for design [9]:

- Minimize the maximum overshoot of the output:

$$f_1 = \max_t |p_{sur} - p_0| \quad (5)$$

- Minimize the settling time of the output: $(|p_{sur} - p_0|) \leq 2\% p_0$.

$$f_2 = t_s \quad (6)$$

These two criteria are used to find the fitness of each individual in the population. Each one of the functions above were transformed and normalized, because we are looking for a minimum, i.e., we want the values of f_1 and f_2 to go towards zero. The fitness function then becomes [9]:

$$f(x) = \sum_{i=1}^2 \left| \frac{r_i - w_i f_i(x)}{r_i} \right| \quad (7)$$

Where r_i is the maximum value allowed for each function and w_i is a weight function. Clearly, in our case, the maximum fitness for an individual will be 2.

In the next section, using some numerical simulations that utilize the described strategy, we will show that the gain matrices can be easily found without any *a priori* analysis of the problem (other than the limits of each coefficient, which are easily distinguishable).

4. SIMULATION RESULTS AND CONCLUSIONS

4.1 Power Transients in RFAs

Here, the power transients are analyzed in Raman amplifiers considering three pump configurations and add/drop of channels in a 16 channels-WDM system using optical fibers DSF and DCF as Raman gain media. The general schematic of the system simulated is shown in the figure below.

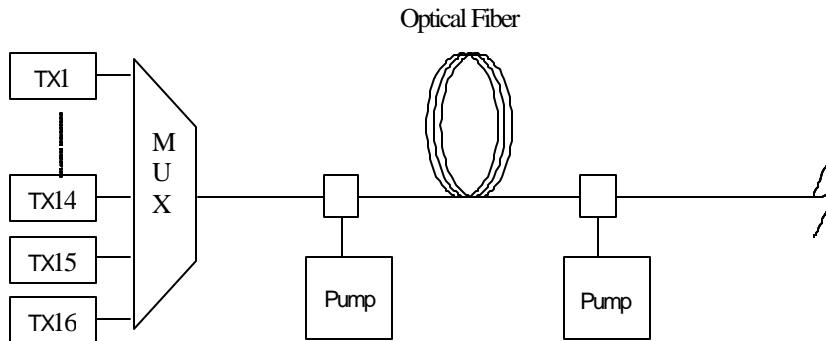


Figure 2 – Raman amplifier system schematic

The attenuation and group delay of the fibers used in the simulation are showed at Fig. 3. The fiber length for the RFAs are 50 km for the DSF, and 10 km for the DCF. The pump in both RFAs was fixed at 1450nm and its total power was 800 mW for the DSF and 200mW for the DCF, for the counter, co-pumped and bi-directional pumped schemes. In the bi-directional pump scheme the power is split at half for each pump laser.

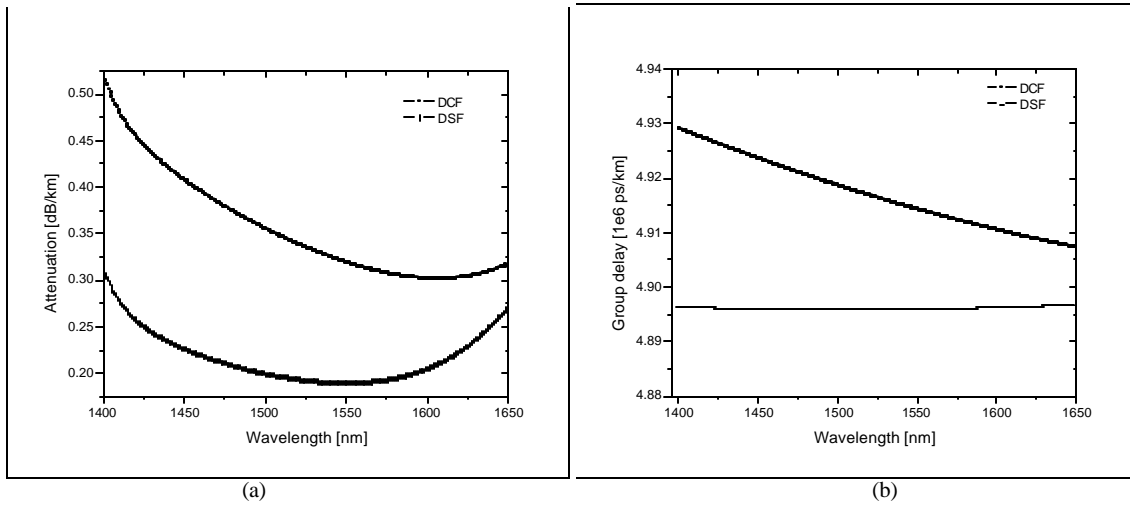


Figure 3 – (a) Attenuation and (b) group delay for the fibers used in the simulations.

The system simulated has 16 channels occupying a bandwidth of 12nm ranging from 1544 nm to 1556 nm and channel spacing equals to 0.8 nm, see Fig. 5(b). Each input signal launches -3dBm optical power into the fiber, what leads the amplifier to operate in a saturation regime. The saturation characteristics of each RFA were analyzed varying the input signal power per channel from -30 dBm to -1 dBm and using the CW RFA model to find the gain for each signal input power.

Fig. 4 shows the gain results found for DSF and DCF fibers for the signal at 1550.4 nm. It is possible to see that the different pump schemes do not cause any large difference in the RFA gain for the DCF fiber and all pump schemes have practically the same gain compression. However, differences are quite considerable when the RFAs using the DSF fiber reach the saturation. In this case the copumped has the largest gain compression and the bi-directional one has an intermediate compression. In general the DSF-RFA presents a stronger saturation than the DCF-RFA that could be explained by the higher pump power of the DSF-RFA [13].

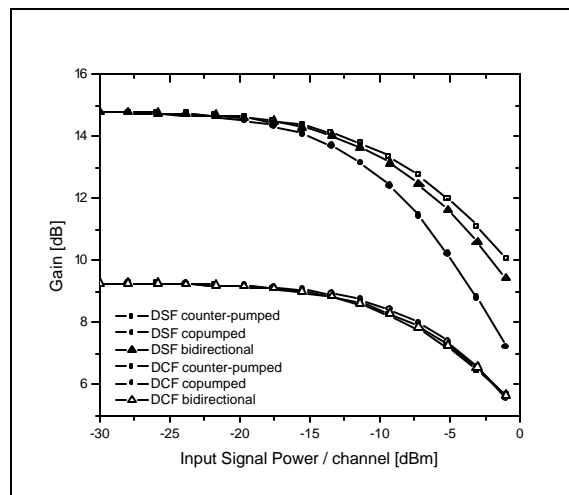


Figure 4 – Gain as function of the input signal power

Some of the channels in the system are 100% square wave modulated to simulate add/drop of channels. Three different patterns were considered here. In the first one, we dropped and then added 2 signals (1544nm and 1556 nm). In the second one, the procedure is repeated with 4 signals (1544 nm, 1544.8 nm, 1555.2 nm and 1556 nm). Finally, in the

third one 8 signals (1544 nm, 1544.8 nm, 1545.6 nm, 1546.4 nm, 1553.6, 1554.4, 1555.2 nm and 1556 nm) are added/dropped. The signals are always dropped at 1.5 ms and added at 2.5 ms. Fig. 5(a) shows the input modulated signal of the channel at 1544 nm.

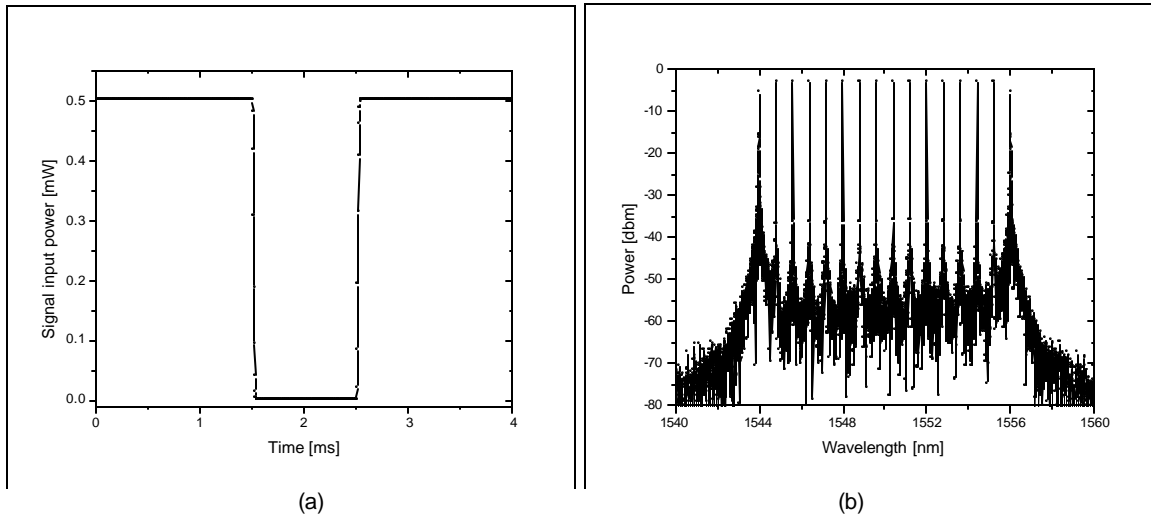


Figure 5 – (a) Modulated signal at 1544 nm to represent the add-drop of channels. (b) Channels distribution.

Before doing the simulations to study the power transients in the RFAs, the output power distribution of this WDM system without the add-drop of channels is found. Fig. 6 shows the output powers; from these values the power excursion is calculated to verify the power evolution of the signals after the add-drop of channels.

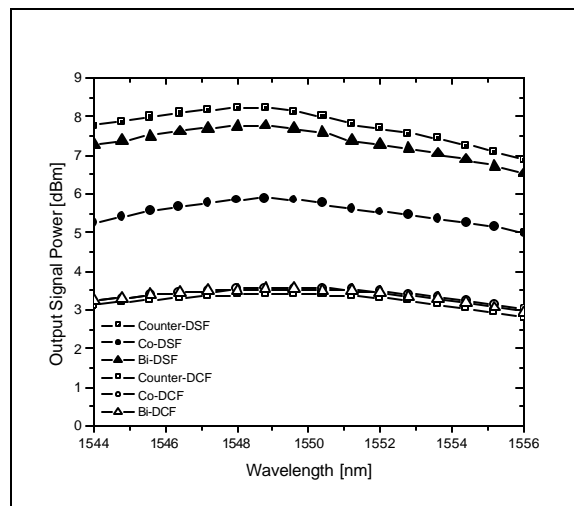


Figure 6 – Output signal power of the 16 channels for the RFAs before the add-drop of channels.

A. DCF-RFA

Figure 7 shows the power excursions on a surviving channel at 1550.4 nm for the RFA counter-pumped when 2, 4 and 8 channels are added-dropped.

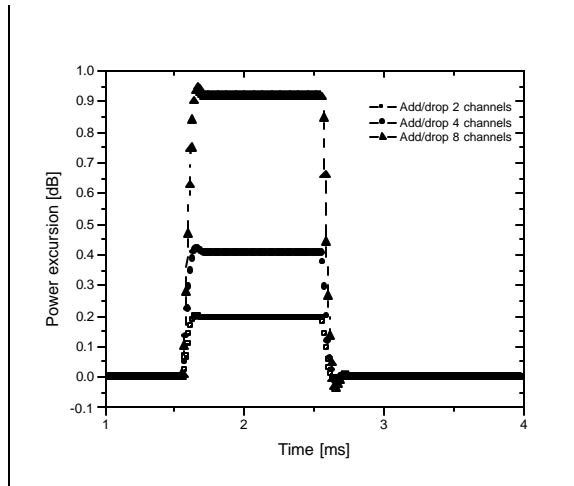


Figure 7 – Output-surviving signal at 1550.4 nm for a DCF counter-pumped.

The leading-edge (drop of channels) in the output signal overshoots and then reaches a new steady-state condition with approximately 0.9 dB higher than the initial condition. In the trailing-edge, (add of channels) the output signal undershoots and then the signal reaches the steady-state condition again. The transients in leading-edge are caused by the lower saturated gain that the surviving channels experience when some channels are dropped. The stronger power in the front signal leads to the depletion of the pump, and the remaining signal does not experience the same gain as in the leading edge due the lower pump power. In the case of the trailing-edge, after the addition of the channels the pump is more depleted, and because it propagates backward, the signal get a lower gain than the steady-state saturated gain.

Unlike the counter-pumped RFA, in the co-pumped configuration the overshoot and undershoot were not noticed, as showed in Fig. 8. Even when the number of add/drop channels was increased, the presence of them was not clearly noticed.

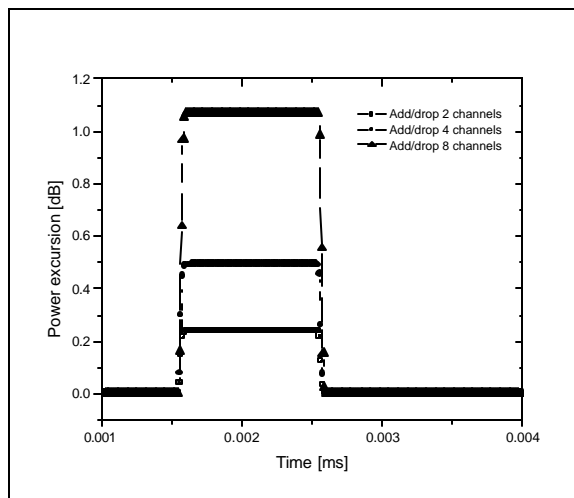


Figure 8 – Output-surviving signal at 1550.4 nm for a DCF copumped.

The transients occur faster in the co-pumped RFA due to the fact that the pump and surviving signals are propagating in the same direction with approximately the same group-velocities.

Finally, the bi-directional pumping scheme seems to have an intermediate response between the co and counter pumped ones (Fig. 9). The overshoot and undershoot are lower than the counter-pumped, but larger than the copumped scheme. Regarding the speed of the transients, we noticed the same pattern: they are faster than the counter-pumped, but not as fast as the copumped RFA.

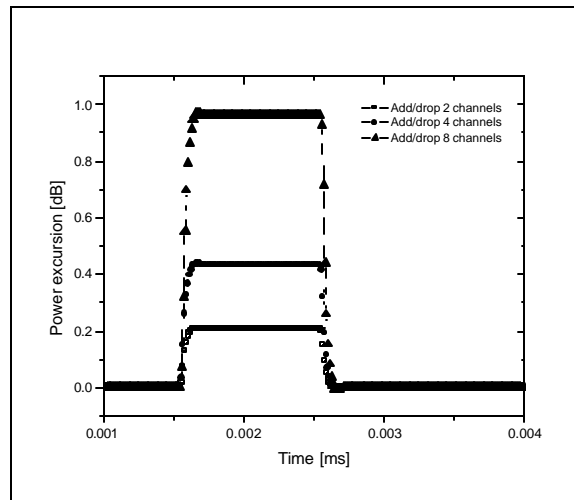


Figure 9 – Output-surviving signal at 1550.4 nm for a DCF bidirectional-pumped.

B. DSF-RFA

Fig. 10 shows the power excursions on surviving channels for the RFA counter-pumped.

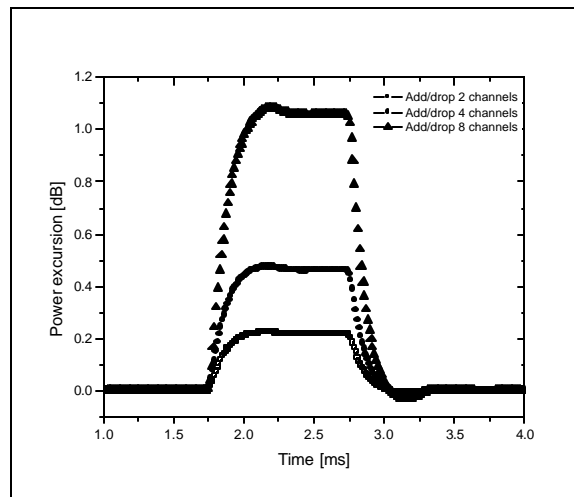


Figure 10 – Output-surviving signal at 1550.4 nm for a DSF counter-pumped.

The curves show the overshoot and undershoot like in the DCF counter-pumped, however, in the DSF case the transients are longer, which could be explained by larger length of fiber [6].

In the co-pumped RFA, Fig. 11, the transient effects present a behavior similar to the one found in the co-pumped DCF case; the transients are very fast and the steady-state condition is soon reached. The power excursion in the copumped RFA is larger than in the counterpumped case. This may be explained by the saturation curves, Fig. 4. The

copumped scheme has larger gain compression and when the channels are dropped it tends to have a larger increase in the gain.

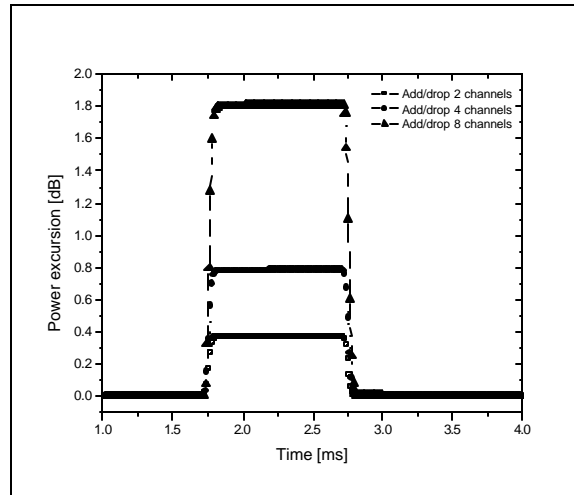


Figure 11 – Output-surviving signal at 1550.4 nm for a DSF co-pumped.

In the bi-directional pumped RFA, the responses Fig. 12, like in the DCF case, are located between the co and counter pumped cases.

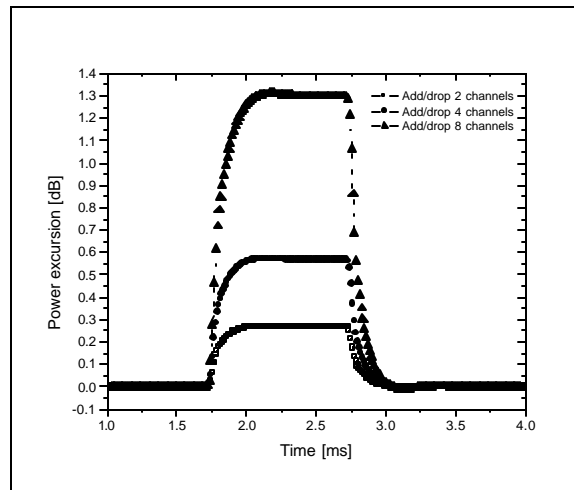


Figure 12 – Output-surviving signal at 1550.4 nm for a DSF bidirectional-pumped.

4.2 Transient Control in RFAs

As demonstrated in the last section, one of the biggest concerns in using optical amplifiers for optical WDM networking is that the networks become vulnerable to transient inter-channel cross-gain modulation while undergoing dynamic configurations. Since optical amplifiers in general, and RFAs in particular, saturate on a total-power basis, addition and/or removal of channels in a WDM network may disturb channels at other wavelengths that share the same path, causing power transients in the surviving channels that could result in serious service impairment. For this reason, a control scheme that reduces the power transients and protects the surviving channels is necessary.

The simulation cases presented here used 40 Km of a DSF fiber as gain medium, this fiber has characteristics similar to the used in last section. In [2], eight signals are propagated with one counter-directional pump. A controller PD with proportional gain, K_P , equal to 10 and differential gain, K_D , equal to 2.4×10^4 is defined.

Using the method based on genetic algorithm described in section 3, after just 15 generations with 20 individuals, a PD controller with $K_P=17.74$ and $K_D=4.83 \times 10^4$ is found within the limits: $0 < K_P < 20$ and $0 < K_D < 10^3$. Fig. 13 shows the results of this last controller when six signals are dropped-added. It should be noticed that it has the same behavior observed in [2], but presents a much better peak and settling time.

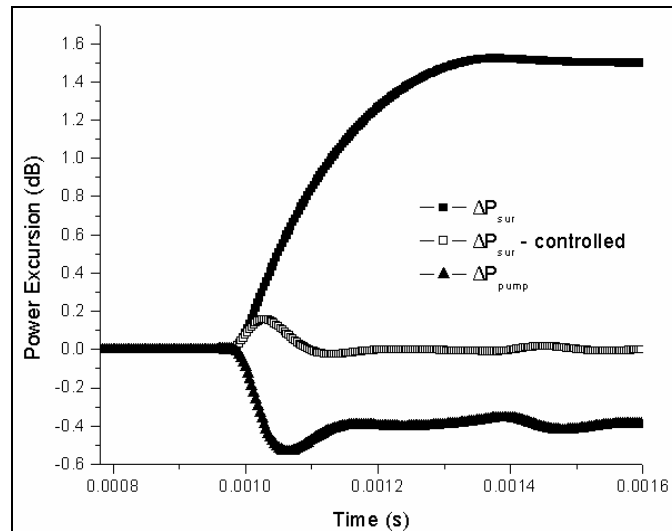


Figure 13 - Power fluctuation for the surviving channel and pump

In the other simulation case, eleven signals, ranging from 1520 nm to 1600 nm with power of 0 dBm/channel, are propagated with four counter directional pumps (1419 nm, 1437nm, 1461, and 1495 nm). In this case four controllers are used, one for each pump, and the parameters were found after 10 generations with 20 individuals each. The power fluctuation for the surviving channel, compared to the case without the controller, is shown in Fig. 14.

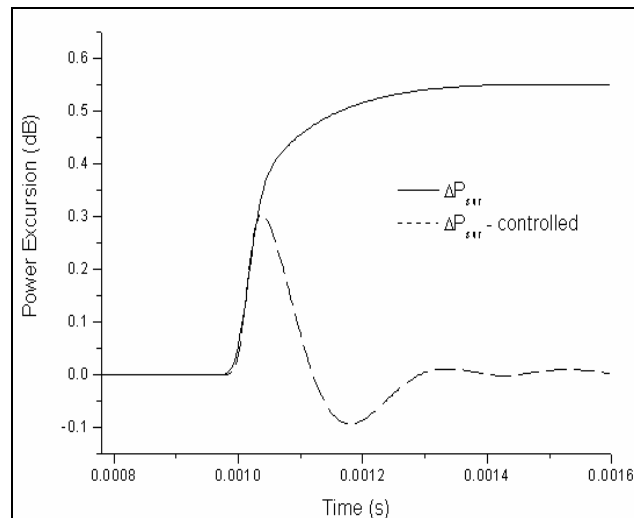


Figure 14 - Power fluctuation for the surviving channel when four pumps are counter-propagated

In this case the results found are not so good as the one presented at Fig. 13, but it could be improved by increasing the number of generations and individuals in the optimization method. Nevertheless, in both simulations, it was observed better control results, using this technique to find the control parameters, than the one used in [2]. For large transients, this technique will help to minimize the impact of power transients in the system performance.

REFERENCES

- [1] M. N. Islam, "Raman Amplifiers for Telecommunications", *J. of Selected Topics in Quantum Electronics*, vol. 8, pp. 548-559, 2002.
- [2] M. Karásek and M. Menif, "Protection of surviving channels in pump-controlled gain-locked Raman fibre amplifier", *Optics Communications*, vol. 210, pp. 57-65, 2002.
- [3] C. Dimopoulos, "Study of dynamic phenomena in WDM optical fibre links and networks based on EDFAs", Doctoral thesis, Department of Electronic Systems Engineering, University of Essex, 2001.
- [4] M. Menif, et. al., "Cross-Gain Modulation in Raman Fiber Amplifier: Experimentation and Modeling", *IEEE Photonics Technology Letters*, vol. 13, no. 9, pp. 1261-1263, 2002.
- [5] M. Freitas, et. al., "Dynamic Behavior in Raman Fiber Amplifiers", XX Simpósio Brasileiro de Telecomunicações, SBT'03, Rio de Janeiro, 2003.
- [6] M. Karásek and M. Menif, "Channel Addition/Removal in Raman Fiber Amplifiers: Modeling and Experimentation", *J. Lightwave Technology*, vol. 20, pp. 1680-1687, 2002.
- [7] W. H. Press, et al., "Numerical Recipes: The Art of Scientific Computing", 2nd Edition, Cambridge University Press, 1992.
- [8] J. G. Ziegler and N. B. Nichols, *Trans. ASME, G, J. Dyn. Sys. Meas. Control* 4 (1942) 759.
- [9] D. H. Kim, "Tuning of PID controller of dead time process using immune based on multiobjective", *Proceedings of the 7th IASTED International Conference ARTIFICIAL INTELLIGENCE AND SOFT COMPUTING*, pp. 368-373, 2003.
- [10] S. Namiki and Y. Emori. "Ultrabroad-band Raman Amplifiers pumped and Gain equalized by Wavelength-Division-Multiplexed high-power lasers". *J. of Selected Topics in Quantum Electronics*, vol. 7, pp. 3-16, 2001.
- [11] Yuhong Kang. "Calculations and Measurements of Raman Gain Coefficients of Different Fiber Types". Master thesis presented at Faculty of the Virginia Polytechnic Institute and State University, 2002.
- [12] S. Givigi, M. Freitas, J. Klein, A. R. de Almeida, and L. C. Calmon. "Transient Control in RFAs for multi-pumping environments by using a multi-objective optimization approach". *Proc. OFC 2004*.
- [13] S. A. E. Lewis, S. V. Chernikov, and J. R. Taylor. "Gain saturation in silica-fibre Raman amplifier". *Electronics Letters*, Vol. 35, pp. 923-924, May 1999.